Journal of Applied Mathematics and Physics, 2021, 9, 2909-2917
https://www.scirp.org/journal/jamp
ISSN Online: 2327-4379
ISSN Print: 2327-4352

Mesoscale Modeling of Hooked-End Steel Fiber Reinforced Concrete under Uniaxial Compression Using Cohesive Elements

Junjie Feng[1], Guansheng Yin[1*], Zhu Liu[2], Jianhong Liang[2], Yunjie Zhang[2], Congge Wen[3]

[1]School of Science, Chang'an University, Xi'an, China
[2]Shaanxi Tietou Engineering Testing Technology Co., Ltd., Xi'an, China
[3]School of Civil Engineering and Architecture, Zhengzhou University of Science and Technology, Zhengzhou, China
Email: fce0814511@163.com, *yings@chd.edu.cn

How to cite this paper: Feng, J.J., Yin, G.S., Liu, Z., Liang, J.H., Zhang, Y.J. and Wen, C.G. (2021) Mesoscale Modeling of Hooked-End Steel Fiber Reinforced Concrete under Uniaxial Compression Using Cohesive Elements. *Journal of Applied Mathematics and Physics*, **9**, 2909-2917.
https://doi.org/10.4236/jamp.2021.911184

Received: August 23, 2021
Accepted: November 20, 2021
Published: November 23, 2021

Abstract

Based on the cohesive zone model, the 2D mesostructures were developed for numerical studies of multi-phase hooked-end steel fiber reinforced concrete under uniaxial compression. The zero-thickness cohesive interface elements were inserted within the mortar, on interfaces of mortar and aggregates and interfaces of mortar and fibers to simulate the failure process of fiber reinforced concrete. The results showed that the numerical results matched well the experimental results in both failure modes and stress-strain behavior. Hooked-end steel fiber reinforced concrete exhibited ductile failure and maintained integrity during a whole failure process. Compared with normal concrete, HES fiber reinforced concrete was greater stiffness and compressive strength; the descending branch of the stress-strain curve was significantly flatter; the residual stress was higher.

Keywords

Fiber Reinforced Concrete, Uniaxial Compression, Cohesive Zone Model, Failure Mode, Stress-Strain Curve

1. Introduction

Fiber reinforced concrete is a multi-phase composite material, which includes coarse and fine aggregates, mortar, fibers, interfaces and porosity, etc. [1]. The micro-cracks begin to appear in a hardening part of the stress-strain curve, and macro-cracks form in a softening branch under the compression. The experiments and numerical simulations show that the failure process is very complex and depends on mesostructure [2]. Meso-mechanical characteristics of concrete

reflect its macro-mechanic response. Specific mesoscale structure, material and internal property may predict the macro-mechanical performance of concrete [2]. The cohesive zone model and extended finite element method, which are low mesh sensitivity and effective convergence, can simulate discrete cracks. Moreover, the cohesive zone model has greater superiority in multi-cracks propagation. There are rarely studies on the mesoscale numerical simulation of fiber reinforced concrete failure process.

The objective of this study is to generate 2D mesostructures with randomly packed aggregates and steel fibers with a volume fraction of 1.5% and investigate the application of the cohesive zone model in fiber reinforced concrete under uniaxial compression.

2. Generation of Mesostructures and Finite Element Models

2.1. Aggregates and Fibers

The coarse aggregates with a continuous gradation of 5 - 20 mm were used, and the mix proportions had been given in [3]. For normal concrete, coarse aggregates represent 40% - 50% of the concrete volume. In this study, the concrete model with 40% aggregate content was adopted. The shape of aggregates is assumed as the circle in the numerical model, which has been accepted and unitized. To reduce computation, the aggregates with diameters ranged from 5 to 20 mm were modeled, and the fine aggregates less than 5 mm merged with cement were treated as mortar. The 2D mesostructure model with dimensions was adopted. The aggregates decomposed into two dimensions follow the classic Walraven function [4]:

$$\begin{aligned} P_c\left(D<D_0\right) = P_k\left(1.065D_0^{0.5}D_{mix}^{-0.5} - 0.053D_0^4D_{mix}^{-4} - 0.012D_0^6D_{mix}^{-6}\right. \\ \left. - 0.0045D_0^8D_{mix}^{-8} + 0.0025D_0^{10}D_{mix}^{-10}\right) \end{aligned} \quad (1)$$

where $P_c\left(D<D_0\right)$ presents the area proportion of aggregates with a particle diameter smaller than D_0; P_k denotes the percentage of the total area of aggregates to the quadrilateral area (about 75% [4]); $D_{\max}$ is the maximum size of aggregates. **Table 1** lists the aggregate size distribution in mesoscale models.

Hooked-end steel (HES) fiber was adopted in this study. **Figure 1** shows the characteristics of HES fiber. The volume fraction of HES fibers is 1.5%. The number (N) of HES fibers in mesoscale models is calculated as follows:

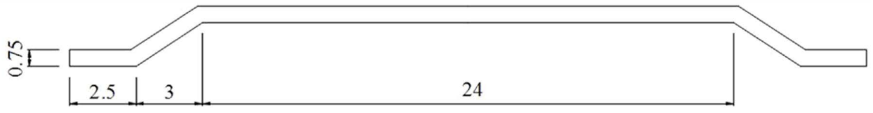

Figure 1. Geometrical characteristics of HES fiber (Unit: mm).

Table 1. Aggregate size distribution in mesoscale models.

Aggregate grain diameter (mm)	5 - 10	10 - 15	15 - 20
Aggregate ratio (%)	19.2%	15.3	5.1%

$$N = round\left(\frac{4\times W\times H\times V_f}{\pi\times d^2\times l}\right) \tag{2}$$

where W and H are the width and height of specimen, respectively; V_f, d and l are the volume fraction, diameter and length of HES fiber, respectively.

2.2. Cohesive Zone Model

The constitutive behavior of zero-thickness cohesive interface element controlled by traction-separation laws was described by the damage initiation criterion and damage evolution law. A bilinear traction-separation law was adopted in this study, illustrated in **Figure 2**.

The damage initiation criterion followed the quadratic nominal stress criterion:

$$\left(\frac{\langle t_n\rangle}{t_n^0}\right)^2+\left(\frac{t_s}{t_s^0}\right)^2=1 \tag{3}$$

where t_n and t_s denote the tractions; t_n^0 and t_s^0 are the critical traction; the $\langle\ \rangle$ is the Macaulay bracket $\langle x\rangle=\begin{cases}x, & x\geq 0\\ 0, & x<0\end{cases}$.

The damage evolution is characterized by a scalar parameter, D. Once the damage criterion is met, all physical mechanisms cause the overall extension of the crack across the elements and the damage parameter D monotonically evolves from 0 (no damage) to 1 (complete damage). The damage parameter D can be formulated by:

$$D=\frac{\delta_m^f\left(\delta_m^{\max}-\delta_m^0\right)}{\delta_m^{\max}\left(\delta_m^f-\delta_m^0\right)} \tag{4}$$

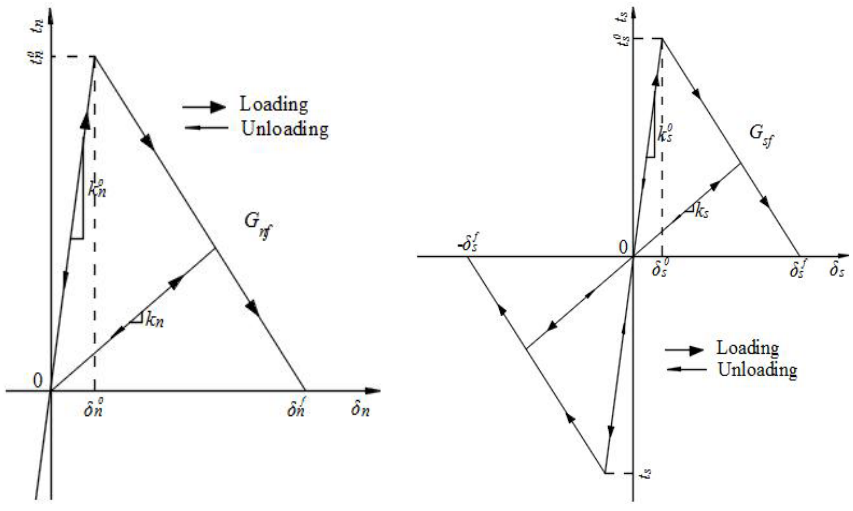

(a) (b)

Figure 2. Bilinear traction-separation law for cohesive element. (a) normal component; (b) shear component.

where δ_m is the effective relative displacement, $\delta_m = \sqrt{\langle \delta_n \rangle^2 + \delta_s^2}$; $\delta_m^{\max}$ is the maximum value of the effective relative displacement attained during the loading history. δ_m^0 is the effective relative displacement at the damage initiation; δ_m^f is the effective relative displacement at failure.

The tractions are affected by damage according to the following equations:

$$t_n = \begin{cases} (1-D)\bar{t}_n, & \bar{t}_n \geq 0 \\ \bar{t}_n, & \bar{t}_n < 0 \end{cases}$$
$$t_s = (1-D)\bar{t}_s \tag{5}$$

where $\bar{t}_n$ and $\bar{t}_s$ are the stress components predicted by the elastic traction-separation behavior for the current strain without damages.

3. Numerical Simulations of the Uniaxial Compression Test

Uniaxial compression tests rectangle specimens were modeled in this study. The area proportion of aggregates and number of HES fibers are met by generating random aggregates and fibers in Digimat software. The solid elements for fibers, aggregates and mortar were assumed to behave linear elastically. Triangle elements provide the most numerous interfaces with the same nodes in the plane and mesh the 2D mesostructures. A 3-node linear triangle plane stress element (CPS3) in ABAQUS is applied to model the fibers, aggregates and mortar. The 4-node two-dimensional cohesive elements (COH2D4) are inserted within the mortar (MII), on interfaces of mortar and aggregates (ITZ_AGG), and on interfaces of mortar and fibers (ITZ_HES) to simulate the stress-strain behavior and failure modes of fiber reinforced concrete. **Figure 3** shows the bulk and cohesive elements creating finite element mesh.

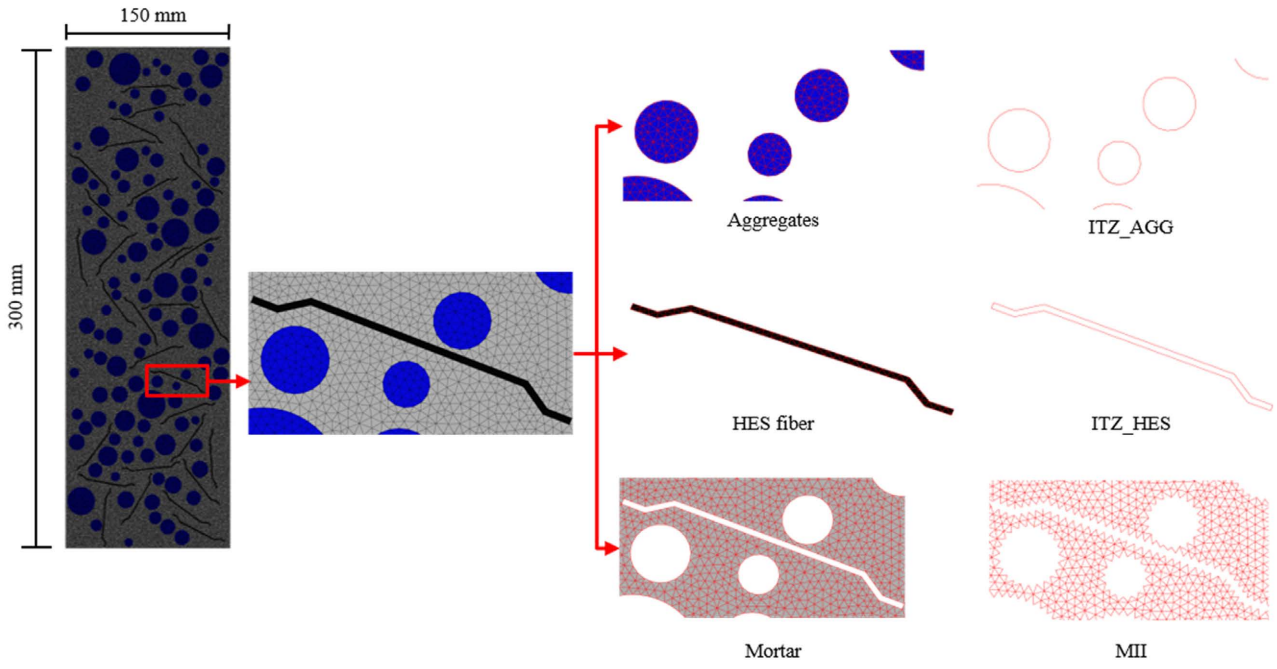

Figure 3. Solid and cohesive elements creating finite element mesh.

All models were fixed at the bottom boundary and subjected to a uniformly distributed displacement at the top boundary, *i.e.*, the displacement-controlled loading scheme was adopted. All analyses were ended at a displacement of 2 mm. Xiong and Xiao [2] indicated that the compressive performance is more sensitive to mesh precision. The model with an element length of 1 mm and loading time of 0.01 s used in the ABAQUS/Explicit solver was validated [5]. Hence, the mesh size of 1 mm was chosen in this study due to its good simulation accuracy and acceptable time consumption.

3.1. Model Parameter

The initial stiffness of cohesive elements, *i.e.*, k_n^0 and k_s^0, are defined for opening and sliding, but the choice of appropriate values is not straightforward. It needs to be high enough to prevent excessive deformations in the elastic regime, but a too high value results in ill-conditioning of the global stiffness matrix. As a guideline for the initial stiffness selection, the relationship between the macro-Poisson ratio and initial stiffness ratio (k_n^0/k_s^0) and the relationship between macro-elastic modulus and initial normal stiffness was proposed by [6]. The trial-and-error method for determining the acceptable initial stiffness was adopted. The ratio of normal to shear properties varies between 2 to 10. The critical traction and fracture energy for normal mode range from 2 to 3 MPa and between 0.01 to 0.1 N/mm, respectively [7].

It is necessary to define the interaction characteristics to simulate the collision and fraction during compression. The friction behavior mainly influences the descending stage of the stress-strain curve and compressive strength. As the suggestion by [6], 0.5 was adopted as an appropriate value for friction coefficient μ. **Table 2** summarizes the material properties.

3.2. Failure Modes

Figure 4 shows the failure modes of the numerical and experimental specimen under the uniaxial compression. The specimens were subjected to the following failure process: after reaching the peak stress, several micro-cracks began to

Table 2. Material properties.

Fiber type	Young's modulus E (GPa)	Poisson's ratio μ	Density ρ (10^{-9} ton/mm^3)	Initial stiffness k_n^0 (MPa/mm)	critical traction t_n^0 (MPa)	Fracture energy G_f (N/mm)
Aggregate	55	0.2	2.6	-	-	-
HES fiber	200	0.3	7.8	-	-	-
Mortar	28	0.2	2.2	-	-	-
ITZ_AGG	-	-	2.2	30,000	3.0	0.1
ITZ_HES	-	-	2.2	30,000	6.0	0.2
MII	-	-	2.2	30,000	6.0	0.5

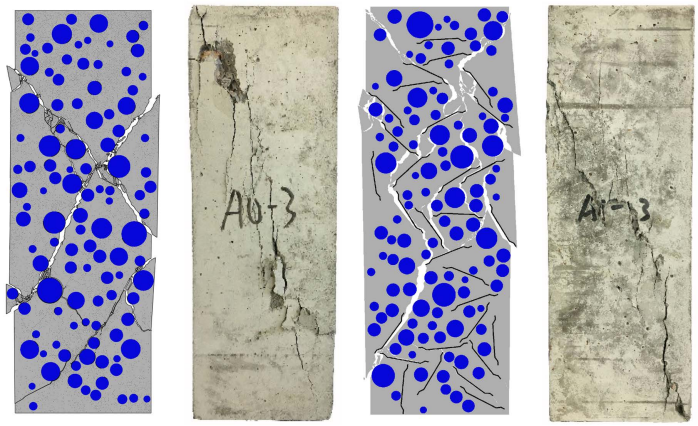

(a) (b)

Figure 4. Failure modes of the numerical specimen and an experimental specimen. (a) Normal concrete; (b) HES fiber reinforced concrete.

appear in the intermediate portion of the specimen, and a major crack was formed gradually upward and downward; finally, the major crack penetrated the surface, failing specimen. For normal concrete, as shown in **Figure 4(a)**, it was observed that the surface of the specimen developed the shear band, and formed the major crack along the diagonal direction. Moreover, the specimen failed in a brittle manner, accompanying peeling off and dislocation and crackling sounds can be heard when the specimen lost bearing capacity. This result was consistent with the previous investigation [8]. The specimens containing HES fibers after failure had more vertical fine cracks. The length and width of the major crack were minor due to the uniform distribution of fibers in the failed interface. The phenomenon may be mainly attributed to the interlocking of fibers, which generates the bridging and confining effect in resisting crack growth, resulting in concrete ductility improvement [9].

3.3. Stress-Strain Curve

As shown in **Figure 5**, the numerical results matched well with experimental curves by the trial-and-error method. Afterward, the cohesive parameters were determined in the mesostructure model, illustrated in **Table 2**. The stress-strain curve of fiber reinforced concrete had similar shapes to normal concrete. Compared with the normal concrete specimen, the slope of ascending branch for specimen with HES fibers was steeper, and the peak stress was greater. It indicated that HES fiber reinforced concrete was greater stiffness and compressive strength. However, the descending branch was significantly flatter than that of mixes without fibers. Due to the addition of fibers, the stress decreased slower after the peak stress, and the residual stress was higher. The result meant that the incorporation of fibers improved the deformability and energy absorption capacity after peak stress. This find is that the concrete matrix has a dominant effect in the ascending branch, while the fibers play their roles in the descending branch and increase the crack resistance [10].

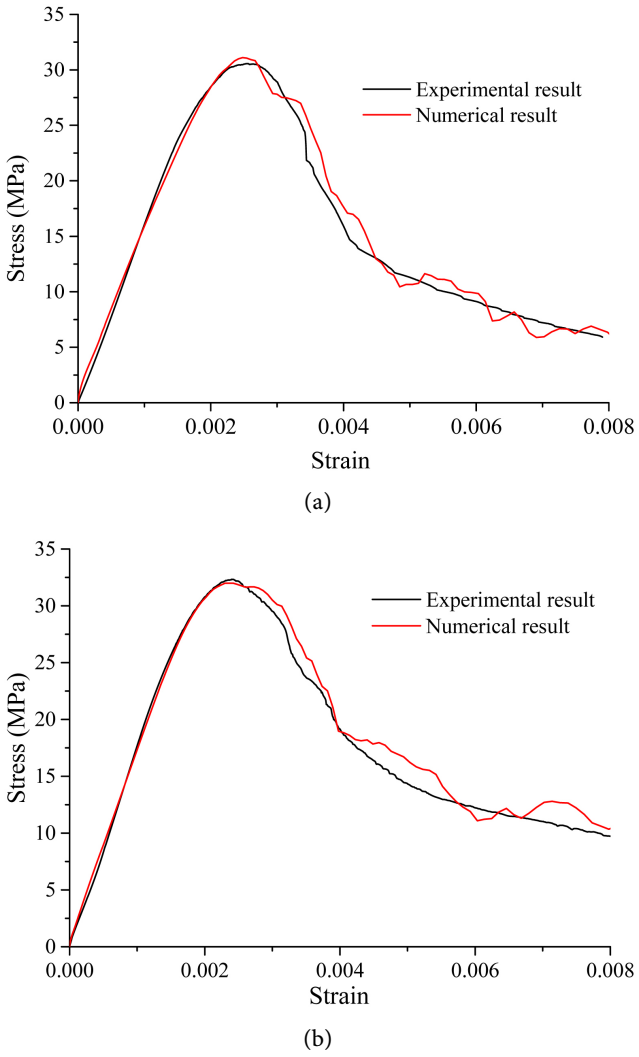

Figure 5. Comparison of the numerical and experimental stress-strain curve. (a) Normal concrete; (b) HES fiber reinforced concrete.

4. Conclusions

The paper has developed the 2D mesostructures of normal concrete and HES fiber reinforced concrete and investigated uniaxial compressive behavior. The following conclusions can be summarized from the numerical and experimental results.

- The failure modes of the numerical specimen are similar to experimental results. Without fibers, the specimen failed in a brittle manner, accompanying peeling off and dislocation. With HES fibers, the specimen developed a group of the wide shear band, exhibited ductile failure, and maintained integrity during a whole failure process.
- The stress-strain curves of the mesostructure model under uniaxial compression matched well with experimental results. Compared with normal concrete, HES fiber reinforced concrete was greater stiffness and compressive strength. The descending branch of specimens with HES fibers was signifi-

cantly flatter, and the residual stress was higher than specimens without fibers.

Acknowledgements

The authors gratefully acknowledge the support of the Fundamental Research Funds for the Central Universities of Chang'an University [grant number 300203211121], the Science and Technology Planning Project in Henan Province of China [grant number 182102311091], the Natural Science Research Project of Zhengzhou Institute of Science and Technology [grant number 2017-XYZK-002].

Conflicts of Interest

The authors declare no conflicts of interest regarding the publication of this paper.

References

[1] Tan, Jin, L., Yu, W., Du, X. and Yang, W. (2020) Meso-Scale Simulations of Size Effect on Concrete Dynamic Splitting Tensile Strength: Influence of Aggregate Content and Maximum Aggregate Size. *Engineering Fracture Mechanics*, **230**, Article No. 106979. https://doi.org/10.1016/j.engfracmech.2020.106979

[2] Xiong, X. and Xiao, Q. (2019) Meso-Scale Simulation of Concrete Based on Fracture and Interaction Behavior. *Applied Sciences*, **9**, Article No. 2986. https://doi.org/10.3390/app9152986

[3] Feng, J., Yin, G., Tuo, H. and Niu, Z. (2021) Parameter Optimization and Regression Analysis for Multi-Index of Hybrid Fiber-Reinforced Recycled Coarse Aggregate Concrete Using Orthogonal Experimental Design. *Construction and Building Materials*, **267**, Article No. 121013. https://doi.org/10.1016/j.conbuildmat.2020.121013

[4] Yu, Y., Zheng, Y. and Zhao, X.Y. (2021) Mesoscale Modeling of Recycled Aggregate Concrete under Uniaxial Compression and Tension Using Discrete Element Method. *Construction and Building Materials*, **268**, Article No. 121116. https://doi.org/10.1016/j.conbuildmat.2020.121116

[5] Wang, X., Yang, Z. and Jivkov, A.P. (2015) Monte Carlo Simulations of Mesoscale Fracture of Concrete with Random Aggregates and Pores: A Size Effect Study. *Construction and Building Materials*, **80**, 262-272. https://doi.org/10.1016/j.conbuildmat.2015.02.002

[6] Qin, C. and Zhang, C. (2011) Numerical Study of Dynamic Behavior of Concrete by Meso-Scale Particle Element Modeling. *International Journal of Impact Engineering*, **38**, 1011-1021. https://doi.org/10.1016/j.ijimpeng.2011.07.004

[7] Wang, J., Jivkov, A.P., Li, Q.M. and Engelberg, D.L. (2020) Experimental and Numerical Investigation of Mortar and ITZ Parameters in Meso-Scale Models of Concrete. *Theoretical and Applied Fracture Mechanics*, **109**, Article No. 102722. https://doi.org/10.1016/j.tafmec.2020.102722

[8] Chen, A., Han, X., Chen, M., Wang, X., Wang, Z. and Guo, T. (2020) Mechanical and Stress-Strain Behavior of Basalt Fiber Reinforced Rubberized Recycled Coarse Aggregate Concrete. *Construction and Building Materials*, **260**, Article No. 119888. https://doi.org/10.1016/j.conbuildmat.2020.119888

[9] Xie, J., Huang, L., Guo, Y., Li, Z., Fang, C., Li, L. and Wang, J. (2018) Experimental Study on the Compressive and Flexural Behaviour of Recycled Aggregate Concrete Modified with Silica Fume and Fibres. *Construction and Building Materials*, **178**, 612-623. https://doi.org/10.1016/j.conbuildmat.2018.05.136

[10] Xie, J., Fang, C., Lu, Z., Li, Z. and Li, L. (2018) Effects of the Addition of Silica Fume and Rubber Particles on the Compressive Behaviour of Recycled Aggregate Concrete with Steel Fibres. *Journal of cleaner production*, **197**, 656-667. https://doi.org/10.1016/j.jclepro.2018.06.237